Graded activation and free energy landscapes of a muscarinic G-protein–coupled receptor

Yinglong Miao[a,b,1] and J. Andrew McCammon[a,b,c,1]

[a]Howard Hughes Medical Institute, University of California, San Diego, La Jolla, CA 92093; [b]Department of Pharmacology, University of California, San Diego, La Jolla, CA 92093; and [c]Department of Chemistry and Biochemistry, University of California, San Diego, La Jolla, CA 92093

Contributed by J. Andrew McCammon, August 31, 2016 (sent for review July 4, 2016; reviewed by Donald Hamelberg and James W. Wells)

G-protein–coupled receptors (GPCRs) recognize ligands of widely different efficacies, from inverse to partial and full agonists, which transduce cellular signals at differentiated levels. However, the mechanism of such graded activation remains unclear. Using the Gaussian accelerated molecular dynamics (GaMD) method that enables both unconstrained enhanced sampling and free energy calculation, we have performed extensive GaMD simulations (~19 μs in total) to investigate structural dynamics of the M_2 muscarinic GPCR that is bound by the full agonist iperoxo (IXO), the partial agonist arecoline (ARC), and the inverse agonist 3-quinuclidinyl-benzilate (QNB), in the presence or absence of the G-protein mimetic nanobody. In the receptor–nanobody complex, IXO binding leads to higher fluctuations in the protein-coupling interface than ARC, especially in the receptor transmembrane helix 5 (TM5), TM6, and TM7 intracellular domains that are essential elements for GPCR activation, but less flexibility in the receptor extracellular region due to stronger binding compared with ARC. Two different binding poses are revealed for ARC in the orthosteric pocket. Removal of the nanobody leads to GPCR deactivation that is characterized by inward movement of the TM6 intracellular end. Distinct low-energy intermediate conformational states are identified for the IXO- and ARC-bound M_2 receptor. Both dissociation and binding of an orthosteric ligand are observed in a single all-atom GPCR simulation in the case of partial agonist ARC binding to the M_2 receptor. This study demonstrates the applicability of GaMD for exploring free energy landscapes of large biomolecules and the simulations provide important insights into the GPCR functional mechanism.

cellular signaling | ligand recognition | protein–protein interactions | allostery | drug discovery

G-protein–coupled receptors (GPCRs) are primary targets of about one-third of currently marketed drugs. They recognize ligands of widely different efficacies, from inverse to partial and full agonists, which transduce cellular signals at differentiated levels. Increasing experimental and computational evidence suggests that GPCRs exist in an ensemble of different conformations that interconvert dynamically during activation and ligand recognition (1–3). The structure, dynamics, and function of GPCRs result from underlying free energy landscapes (4). However, quantitative characterization of the GPCR activation and ligand-dependent free energy profiles has proved challenging (4–12).

The M_2 muscarinic GPCR is widely distributed in mammalian tissues. It plays a key role in regulating the human heart rate and heart contraction forces. The M_2 receptor has been crystallized in both an inactive state bound by the inverse agonist 3-quinuclidinyl-benzilate (QNB) (13) and an active state bound by the full agonist iperoxo (IXO) and a G-protein mimetic nanobody (14). The receptor activation is characterized by rearrangements of the transmembrane (TM) helices 5, 6, and 7, particularly closing of the ligand-binding pocket, outward tilting of the TM6 cytoplasmic end, and close interaction of $Tyr206^{5.58}$ and $Tyr440^{7.53}$ in the G-protein–coupling site (14). The residue superscripts denote the Ballesteros–Weinstein (BW) numbering of GPCRs (15).

In addition to binding inverse and full agonists, the M_2 receptor recognizes partial agonists that often possess lower affinities and elicit submaximal activity (16). Coupling of the receptor with the G protein or mimetic nanobody typically increases agonist binding affinities (17). However, structural information of partial agonist binding is scarce, except for few other GPCRs (18). How can one GPCR accommodate chemically diverse ligands? What are the structural signatures underlying the binding of different ligands? Why do some partial agonists exhibit lower binding affinities than full agonists? Is it easier for partial agonists to dissociate from the receptor? What are the pathways of ligand dissociation and binding? Because the partial agonists elicit only submaximal activity of GPCRs, do they stabilize different receptor conformations? It is important to address these questions to elucidate the GPCR functional mechanism.

Using Gaussian accelerated molecular dynamics (GaMD) simulations that enable both unconstrained enhanced sampling and free energy calculation (19), here we investigate structural dynamics of the M_2 receptor that is bound by the full agonist IXO, the partial agonist arecoline (ARC), and the inverse agonist QNB, in the presence or absence of the G-protein mimetic nanobody Nb9-8 (Table S1). Upon binding of different ligands, the receptor exhibits distinct flexibility and free energy profiles in the orthosteric pocket, the extracellular vestibule, and the intracellular G-protein–coupling site, for which the sizes are characterized by the perimeter of triangle formed by the C_α atoms of $Tyr104^{3.33}$–$Tyr403^{6.51}$–$Tyr426^{7.39}$ or "tyrosine lid" (14), the distance between the C_α atoms of Tyr177 in extracellular loop 2 (ECL2) and $Asn410^{6.58}$, and the C_α atom distance between $Arg121^{3.50}$ and $Thr386^{6.34}$, respectively. The receptor orthosteric pocket samples distinct closed and open conformations, and the G-protein–coupling site interconverts between the inactive, intermediate, and fully active states. We have observed both dissociation and binding of an orthosteric ligand in a GPCR all-atom simulation. Therefore, we are able to obtain a detailed picture of GPCR graded activation.

Significance

G-protein–coupled receptors (GPCRs) represent primary targets of about one-third of currently marketed drugs. The structure, dynamics, and function of GPCRs result from complex free energy landscapes. In this work, we have applied Gaussian accelerated molecular dynamics (GaMD) to study the ligand-dependent behavior of the M_2 muscarinic GPCR. Extensive GaMD simulations have revealed distinct structural flexibility and free energy profiles that depict graded activation of the M_2 receptor. We have captured both dissociation and binding of an orthosteric ligand in a single all-atom GPCR simulation. GaMD is well poised to study large biomolecules and ligand recognition for drug discovery.

Author contributions: Y.M. and J.A.M. designed research; Y.M. performed research; Y.M. analyzed data; and Y.M. and J.A.M. wrote the paper.

Reviewers: D.H., Georgia State University; and J.W.W., University of Toronto.

The authors declare no conflict of interest.

[1]To whom correspondence may be addressed. Email: yimiao@ucsd.edu or jmccammon@ucsd.edu.

This article contains supporting information online at www.pnas.org/lookup/suppl/doi:10.1073/pnas.1614538113/-/DCSupplemental.

Results

Agonist-Dependent Flexibility and Free Energy Profiles of the Nanobody-Coupled Receptor. In the presence of the G-protein mimetic nanobody, the M_2 receptor exhibits varied structural flexibility when the ligand is changed from full agonist IXO to partial agonist ARC (Fig. 1*A*). Binding of ARC leads to significantly increased fluctuations in the ECL2 and orthosteric pocket. This is consistent with the fact that ARC possesses lower affinity than IXO (14, 16, 20). Thus, weaker interaction is formed between ARC and the receptor. Surprisingly, opposite flexibility change was observed in the receptor intracellular half. Binding of IXO leads to higher fluctuations in the G-protein–coupling interface, especially in the TM5, TM6, and TM7 intracellular domains, which have been shown as essential elements for activation of GPCRs (1). Therefore, increased flexibility of the receptor intracellular domains upon full agonist binding apparently contributes to GPCR activation.

Potential of mean force (PMF) calculations showed that the IXO-nanobody–bound M_2 receptor is confined in a local energy well centered at (14.5 Å, 13.5 Å) in the C_α atom distances between $Arg121^{3.50}$–$Thr386^{6.34}$ and $Tyr177^{ECL2}$–$Asn410^{6.58}$ (Fig. 1*B* and Fig. S1). The receptor maintains the active X-ray conformation through GaMD simulations. The distance between the ligand-charged N atom and the C_γ atom of $Asp103^{3.32}$ adopts a free energy minimum at 4.5 Å (same as the X-ray conformation) (Fig. 1*C*). The tyrosine lid exhibits an energy minimum at 30 Å, being similar to 29.7 Å in the closed X-ray conformation (Fig. 1*C*).

In comparison, the ARC-nanobody–bound M_2 receptor exhibits a narrower energy well in the $Arg121^{3.50}$–$Thr386^{6.34}$ distance than the IXO-nanobody–bound form (Fig. 1*D*). This result is consistent with the above finding that changing the ligand from IXO to ARC leads to reduced flexibility in the receptor intracellular domains. On the other hand, the tyrosine lid explores a larger conformational space with weaker binding of ARC (Fig. 1*E*). ARC samples two low-energy conformations, "ARC-P1" (Fig. 1*F*) and "ARC-P1′" (Fig. 1*G*), for which the preferred distances between ARC and $Asp103^{3.32}$ are 3.5 Å and 5.5 Å, respectively (Fig. S2). The ARC-P1′ pose is closely similar to that obtained from Glide docking. ARC forms weaker interaction with the M_2 receptor than IXO and exhibits dynamic binding.

Ligand-Dependent Dynamics of the Nanobody-Free Receptor. Removal of the G-protein mimetic nanobody leads to deactivation of the M_2 receptor even with agonist binding. This is reflected by decreased distances between $Arg121^{3.50}$ and $Thr386^{6.34}$ in GaMD simulations of the M_2-ARC and M_2-IXO complexes (Figs. S3 and S4). The receptor in these two complexes is more flexible than in the QNB-bound form (Fig. 2 *A*–*C* and Fig. S5). The IXO-bound receptor exhibits lower flexibility in the extracellular vestibule, but higher fluctuations in the TM5, TM6, and TM7 intracellular domains than the ARC-bound form (Fig. S6), being similar to the nanobody-bound complexes (Fig. S7). Moreover, ARC undergoes significantly higher fluctuations than IXO (Fig. 2 *B* and *C*).

In the QNB-bound receptor, the $Tyr177^{ECL2}$–$Asn410^{6.58}$ distance exhibits a free energy minimum at 14.5 Å, similar to 15.9 Å in the X-ray structure (13). Binding of the smaller agonists ARC and IXO shrinks the extracellular vestibule to an energy minimum distance of 12.5 Å between $Tyr177^{ECL2}$ and $Asn410^{6.58}$, although with fluctuations (Fig. 2 *E* and *F*). On the intracellular side, the global energy minimum is identified for the nanobody-free receptor in the inactive state with ∼6–7 Å distance between $Arg121^{3.50}$–$Thr386^{6.34}$. Additional low-energy states are also observed with outward movement of the TM6 cytoplasmic end at differentiated magnitudes. Upon binding IXO, the receptor samples two intermediate states with the $Arg121^{3.50}$–$Thr386^{6.34}$ distance centered at 10.0 Å ("I1") and 12.0 Å ("I2"), respectively (Fig. 2*F*). In comparison, only the intermediate I1 appears in PMF of the ARC-bound receptor in addition to the inactive state (Fig. 2*E*). Although agonists alone could not open the intracellular pocket up to the fully active state, IXO binding leads to greater movement of the TM6 cytoplasmic end than ARC.

Upon binding QNB, the receptor tyrosine lid is confined to the X-ray conformation (Fig. 2*G*). QNB remains tightly bound to the orthosteric site through the GaMD simulations. In contrast, the full and partial agonists allow the receptor to sample a significantly larger conformational space in the tyrosine lid (Fig. 2 *H* and *I*). IXO is able to escape out of the orthosteric pocket in one of the GaMD simulations, visiting the extracellular vestibule with 12.5 Å distance between ligand and $Asp103^{3.32}$ (Fig. 2*I* and Fig. S8). In the case of ARC, not only does it escape out of the orthosteric pocket, but also it dissociates completely and rebinds repeatedly to the

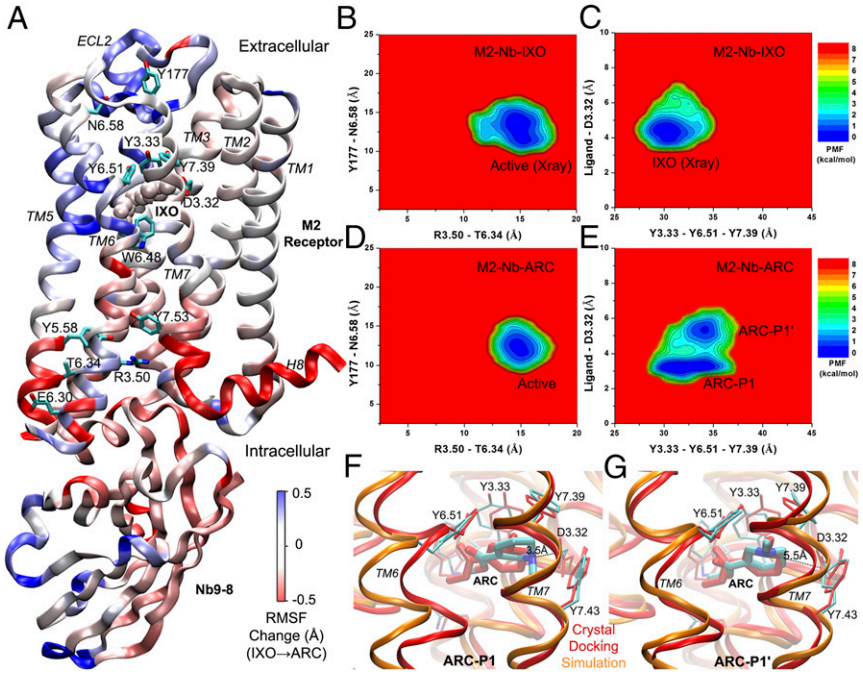

Fig. 1. Structural flexibility and free energy profiles of the M_2 receptor bound by the G-protein mimetic nanobody Nb9-8 and full agonist IXO or partial agonist ARC. (*A*) Schematic representation of the IXO-nanobody–bound M_2 receptor [Protein Data Bank (PDB) ID code 4MQS] that is colored by root-mean square fluctuation (RMSF) differences when the ligand is changed from IXO to ARC. A color scale of –0.5 Å (red) to 0.5 Å (blue) is used. The proteins are shown in ribbons and ligand in spheres. Important residues are represented by sticks and labeled with the BW numbers except Tyr177 in ECL2. (*B* and *C*) Two-dimensional PMF profiles of the M_2-nanobody–IXO system regarding (*B*) the $Arg121^{3.50}$–$Thr386^{6.34}$ and $Tyr177^{ECL2}$–$Asn410^{6.58}$ distances and (*C*) the $Tyr104^{3.33}$–$Tyr403^{6.51}$–$Tyr426^{7.39}$ triangle perimeter and the ligand–$Asp103^{3.32}$ distance. (*D* and *E*) The corresponding 2D PMF profiles of the M_2-nanobody–ARC system. (*F* and *G*) Two dominant binding poses of ARC in the orthosteric site: (*F*) ARC-P1 and (*G*) ARC-P1′. ARC is shown in thick sticks, the receptor in orange ribbons, and the interacting protein residues in thin sticks. The docking conformation of ARC in the 4MQS crystal structure is also shown in red for comparison.

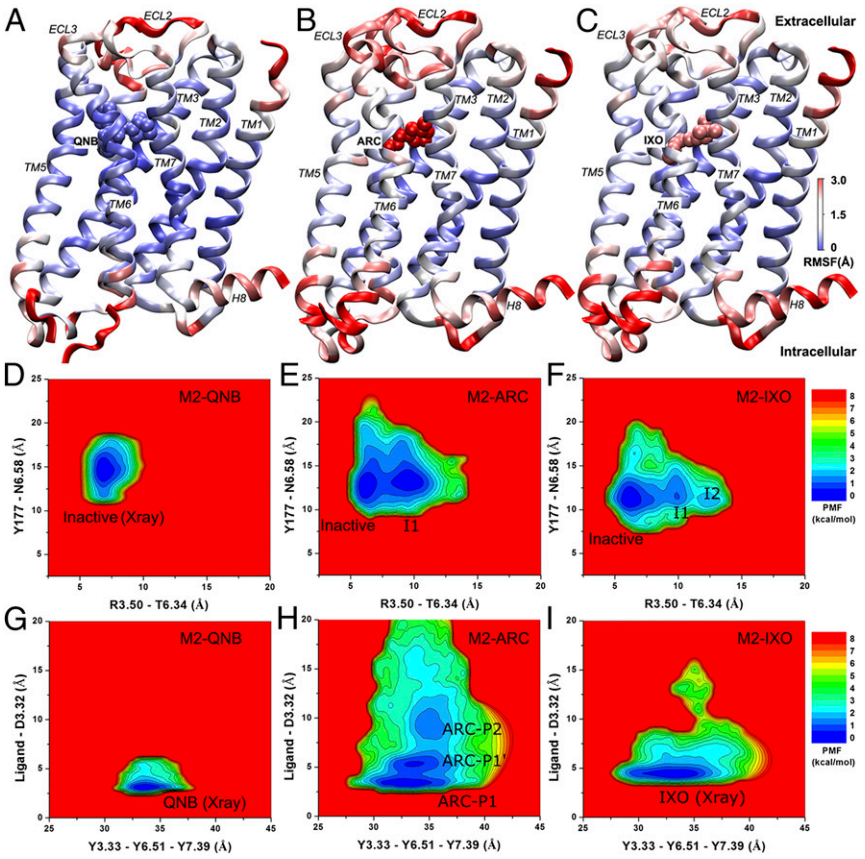

Fig. 2. Structural flexibility and free energy profiles of the M_2 receptor bound by the inverse agonist QNB, partial agonist ARC, and full agonist IXO, in the absence of the G-protein mimetic nanobody. (*A*–*C*) Schematic representations of the (*A*) M_2-QNB, (*B*) M_2-ARC, and (*C*) M_2-IXO complex structures colored by the protein/ligand RMSFs with a scale of 0 Å (blue) to 3 Å (red). The protein is shown in ribbons and ligands in spheres. (*D*–*F*) Two-dimensional PMF profiles of the Arg121$^{3.50}$–Thr386$^{6.34}$ and Tyr177^{ECL2}–Asn410$^{6.58}$ distances for the (*D*) M_2-QNB, (*E*) M_2-ARC, and (*F*) M_2-IXO systems. Distinct conformational states of the M_2 receptor identified in the low-energy wells, including the inactive and intermediates I1 and I2, are labeled and shown in Fig. 3. (*G*–*I*) Two-dimensional PMF profiles of the Tyr104$^{3.33}$–Tyr403$^{6.51}$–Tyr426$^{7.39}$ triangle perimeter and ligand–Asp103$^{3.32}$ distance for the (*G*) M_2-QNB, (*H*) M_2-ARC, and (*I*) M_2-IXO systems. Different binding poses of the ligands identified in the low-energy wells are labeled, particularly ARC-P1, ARC-P1′, and ARC-P2 (corresponding to cluster C2 in Fig. 4 that is located in the receptor extracellular vestibule).

receptor (described in more detail below). The distance between ARC and Asp103$^{3.32}$ samples different low-energy states at 3.5 Å (ARC-P1), 5.5 Å (ARC-P1′), and ∼10 Å (ARC-P2) (Fig. 2*H*). This finding presumably results from weaker binding of ARC compared with IXO and QNB (14, 16, 20).

Low-Energy Conformational States of the M_2 Receptor. Through this study, distinct low-energy states are identified from free energy profiles of the M_2 receptor upon binding of different ligands. The orthosteric pocket exhibits both closed and open conformations (Fig. 3*A*), for which the tyrosine lid samples free energy minima at ∼30 Å and ∼33 Å, respectively (Fig. 3*C*). In the presence of the G-protein mimetic nanobody, IXO shifts the receptor conformational equilibrium to the closed state. In contrast, ARC allows the orthosteric pocket to sample both the closed and open states. Without the nanobody, QNB confines the receptor orthosteric pocket in the open state. ARC and IXO, however, yield a significantly broader energy well covering both the open and closed states although the open state is favored.

The G-protein–coupling site samples the inactive, intermediates I1 and I2, and active conformational states (Fig. 3*B*), for which low-energy minima are found for the Arg121$^{3.50}$–Thr386$^{6.34}$ distance at 6.0–7.0 Å, ∼10 Å, ∼12 Å, and ∼15 Å, respectively (Fig. 3*D*). QNB confines the receptor in the inactive state, whereas binding of IXO and ARC, along with the nanobody, shifts the receptor to the fully active state. In contrast, the full/partial agonist alone allows the receptor to sample more than one low-energy state. The M_2-ARC complex samples the inactive and intermediate I1 states with similar free energies. In addition, IXO shifts the conformational equilibrium further and allows the receptor to visit the intermediate I2 state.

Pathways of Ligand Dissociation and Binding. During the 2,030-ns GaMD simulation of the M_2-ARC system (Table S1), ARC was observed to dissociate completely and rebind to the receptor multiple times as indicated by the time course of the ligand–Asp103$^{3.32}$ distance (Fig. 4*A* and Movie S1). Four dissociation (denoted "D1," "D2," "D3," and "D4") and three binding (denoted "B1," "B2," and "B3") events took place. ARC exited the receptor via three extracellular openings, one formed between ECL2 and ECL3 (D1, Fig. 4*B*), the second between ECL2 and TM2 and TM7 (D2, Fig. 4*F*), and the third between ECL2 and TM7 (D3 and D4, Fig. 4 *G* and *H*). ARC rebound to the receptor through two of the three openings, i.e., ECL2/ECL3 (B1, Fig. 4*C*) and ECL2/TM7 (B2 and B3, Fig. 4 *E* and *G*).

To obtain a quantitative picture of the ligand-binding pathways, the density-based spatial clustering of applications with noise (DBSCAN) algorithm (21) was applied to cluster trajectory snapshots of the ligand by combining all 10 GaMD simulations of M_2-ARC (total 9,100 ns). Energetic reweighting (19, 22) was then performed on each of the ligand clusters to recover the original free energy (details in *SI Methods*). Ten ligand clusters with the lowest free energies are shown in Fig. 4*I*. A global energy minimum (0 kcal/mol) is found for cluster "C1" in the orthosteric pocket. The second-lowest energy is identified for cluster "C2" (1.34 kcal/mol) at the center of the extracellular vestibule between ECL2 and TM7. Two clusters of higher energies, "C3" with 2.01 kcal/mol and "C4" with 2.29 kcal/mol, appear to connect C1 in the orthosteric pocket and C2 in the extracellular vestibule. A cavity formed by the extracellular domains of TM3/TM2/TM7 is filled with two clusters, "C5" (2.33 kcal/mol) and "C8" (2.69 kcal/mol). Similarly, another cavity formed by the TM4/TM5/TM6 extracellular domains is filled with clusters "C7" and "C9" with 2.49 kcal/mol and 3.15 kcal/mol free energies, respectively. In the extracellular vestibule, although ARC was observed to exit between ECL2 and TM2 and TM7 in one of the dissociation events, this location does not appear among the 10 lowest-energy clusters. In contrast, two energetically favored clusters are found in the opening between ECL2 and ECL3, i.e.,

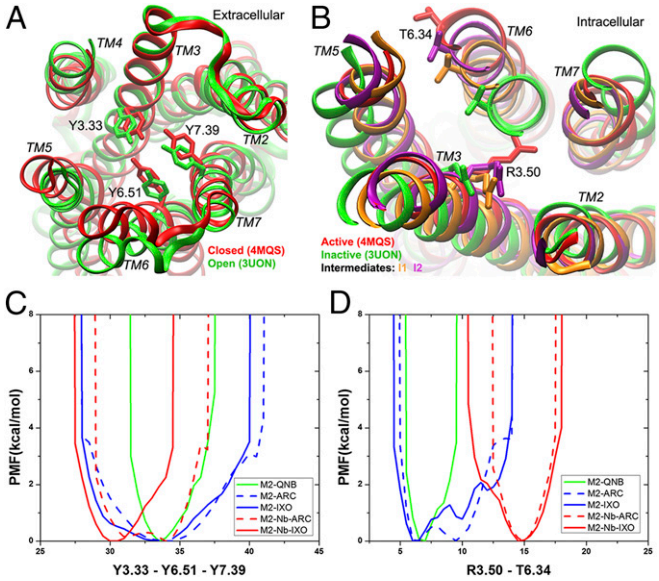

Fig. 3. Distinct low-energy states sampled by the M_2 receptor in the orthosteric ligand-binding and intracellular G-protein–coupling sites. (*A*) The orthosteric site exhibits closed (red, 4MQS X-ray) and open (green, 3UON X-ray) conformations. (*B*) The G-protein–coupling site samples inactive (green, 3UON X-ray), intermediates I1 (orange) and I2 (purple), and active (red, 4MQS X-ray) conformational states. (*C* and *D*) The 1D PMF profiles of (*C*) the Tyr104$^{3.33}$–Tyr403$^{6.51}$–Tyr426$^{7.39}$ triangle perimeter and (*D*) the Arg121$^{3.50}$–Thr386$^{6.34}$ distance calculated for the M_2-QNB, M_2-ARC, M_2-IXO, M_2-nanobody–ARC, and M_2-nanobody–IXO complex systems.

"C6" (2.36 kcal/mol) and "C10" (3.22 kcal/mol). Therefore, clusters C1 ↔ C3 ↔ C4 ↔ C2 ↔ C10 ↔ C6 appear to represent an energetically preferred pathway for ARC dissociation and binding. IXO also follows a similar pathway during dissociation from the orthosteric site to the ECL2/ECL3 opening and rebinding to the center of the extracellular vestibule (Fig. S8 and Movie S2).

Discussion

In this study, detailed ligand-dependent dynamics and free energy profiles of the M_2 muscarinic GPCR have been obtained through extensive GaMD simulations (~19 us in total). The energy minimum states identified from GaMD simulations of the QNB-bound and the IXO-nanobody–bound receptor are the same as the inactive and fully active receptor X-ray structures (13, 14), respectively. The simulations also revealed new low-energy states in the IXO/ARC-bound receptor upon removal the nanobody. Whereas the inverse agonist QNB with high binding affinity (~0.06 nM) (14) remains tightly bound to the orthosteric site, the full and partial agonists with lower affinities, ~5 μM for ARC (16, 20) and ~0.01 μM for IXO (14), exhibit significantly higher fluctuations. We have captured both dissociation and binding of an orthosteric ligand in a single all-atom GPCR simulation in the case of ARC binding to the M_2 receptor. These results are consistent with the recent experimental finding that the G-protein mimetic nanobody stabilizes a closed receptor conformation and dramatically affects the association and dissociation of GPCR ligands (17). Notably, Dror et al. (23) successfully observed both binding and dissociation of allosteric modulators at the M_2 receptor through long-timescale conventional MD (cMD) simulations. However, the allosteric site is located in the receptor extracellular vestibule, ~15Å above the deeply buried orthosteric site. It is also important to note that a direct link between the binding affinity of individual GPCR ligands and their efficacy is still lacking (16, 20, 24). Whereas ARC exhibits lower affinity than IXO or QNB as investigated in the present study, certain partial agonists are not necessarily weaker binders compared with full or inverse agonists (16, 24). Nevertheless, there appears to be a correlation between efficacy and the breadth of the dispersion of affinities for agonists of the M_2 receptor (16, 20, 25). The GaMD simulations provided important insights into the binding mechanism of three studied ligands and GPCR graded activation.

Overall, the M_2 receptor samples a large conformational space (Fig. 5). In the presence of the G-protein mimetic nanobody, the receptor is stabilized in the fully active state with the most open intracellular pocket and the narrowest extracellular vestibule. In the orthosteric pocket, IXO stabilizes the receptor in the closed state, whereas ARC binding allows the receptor to change between the closed and open states with two alternative poses (ARC-P1 and ARC-P1′). Such dynamic binding of the partial agonist, along with multiple associated receptor conformations, has previously been observed in NMR experiments of the peroxisome proliferator-activated receptor γ (26).

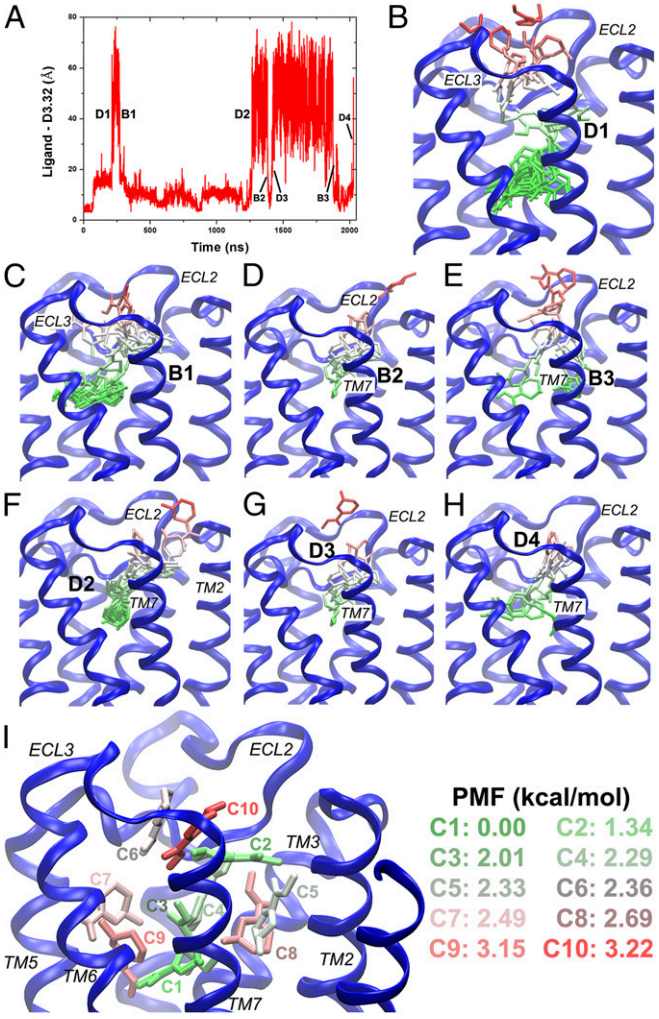

Fig. 4. Pathways of partial agonist dissociation and binding observed in GaMD simulation. (*A*) Time course of the ARC–Asp103$^{3.32}$ distance during 2,030-ns simulation. Four dissociation and three binding events are labeled. (*B–H*) Schematic representations of the ligand pathways during (*B*) D1, (*C*) B1, (*D*) B2, (*E*) B3, (*F*) D2, (*G*) D3, and (*H*) D4. The receptor is represented by blue ribbons and the ligand by sticks colored by the position along the membrane normal. (*I*) Ten lowest-energy structural clusters of ARC that are labeled and colored in a Green–White–Red (GWR) scale according to the PMF values.

Removal of the nanobody leads to deactivation of the M_2 receptor with inward displacement of the TM6 cytoplasmic end. This is consistent with extensive experimental and computational studies of GPCRs, especially on the β_2-adrenergic receptor (β_2AR) (6). Binding of QNB confines the receptor in the inactive state with the shortest distance between $Arg121^{3.50}$ and $Thr386^{6.34}$ (~6–7 Å). Without the G-protein or mimetic nanobody, ARC biases the receptor to visit an intermediate state I1 that exhibits increased distance between $Arg121^{3.50}$ and $Thr386^{6.34}$ (~10 Å). In comparison, IXO is able to bias the receptor further, sampling both intermediates I1 and I2 with ~10 Å and ~12 Å distances between $Arg121^{3.50}$ and $Thr386^{6.34}$, respectively. Note that our earlier accelerated MD (aMD) simulations captured a similar conformational change during activation of the apo M_2 receptor that exhibits basal activity (12). Even without agonist binding, the apo receptor undergoes transient outward movement of the TM6 cytoplasmic end up to ~12 Å. To a certain extent, the intermediate I2 in the present study can be considered an "active-like" state, which has been used to define the agonist-bound adenosine A_{2A} receptor (A_{2A}AR) (27). In summary, graded activation of the M_2 receptor is characterized by outward movement of the TM6 cytoplasmic end at increasing magnitudes when the ligand changes from inverse to partial and full agonists.

The orthosteric pocket samples two distinct conformations, being open in the QNB-bound M_2 receptor (13) and closed in the IXO-nanobody–bound form (14). It interconverts dynamically between the closed and open states when the ligand is changed from IXO to ARC in the nanobody-coupled receptor (Fig. 3*C*), although the extracellular vestibule remains to adopt the narrowest opening (Fig. S9*B*). It also exhibits a broad energy well covering both the closed and open states in the M_2-IXO and M_2-ARC complexes. Given such plasticity, the orthosteric pocket of the M_2 receptor is able to accommodate different ligands of various sizes (14, 16). In addition, the extracellular vestibule in the IXO- and ARC-bound receptor samples both the narrow and wide opening conformations, for which the distances between $Tyr177^{ECL2}$ and $Asn410^{6.58}$ are 12.5 Å and ~16 Å, respectively(Fig. 2 and Fig. S9). Overall, the extracellular vestibule appears highly flexible. Binding of allosteric modulators may stabilize it in specific conformations and alter the orthosteric ligand-mediated responses (14, 23).

In earlier computational studies, ligand-dependent dynamics of GPCRs were investigated using the cMD (7, 10), metadynamics (8, 9), and aMD (11) methods. Whereas cMD simulations revealed distinct conformational changes in several known GPCR activation elements (7), these simulations lasting several hundred nanoseconds were not long enough to capture the entire GPCR activation/deactivation processes. For the β_2AR, cMD simulations were combined with coarse-grained modeling to sample the receptor ensemble conformations (10). Moreover, metadynamics were used to characterize free energy landscapes of the β_2AR (8) and A_{2A}AR (9). However, metadynamics require predefined collective variables and may constrain the dynamic GPCR activation or deactivation pathways. Recently, we applied aMD to simulate binding of different ligands to the M_3 muscarinic receptor (11). Although the aMD simulations successfully captured binding of the partial and full agonists without constraints, the boost potential suffered from large energetic noise and precluded accurate reweighting to recover the original free energy landscapes. By constructing boost potential that follows a Gaussian distribution, GaMD enabled simultaneous unconstrained enhanced sampling and free energy calculations. It allows for detailed characterization of the ligand-dependent dynamics of the M_2 receptor.

During one of the GaMD simulations, IXO with ~0.01 μM affinity escapes out of the orthosteric pocket and visits the extracellular vestibule (Fig. S8 and Movie S2). For ARC with 5.0 μM binding affinity, not only does it escape out of the orthosteric pocket, but also it dissociates completely and rebinds to the receptor repeatedly during a 2,030-ns GaMD simulation

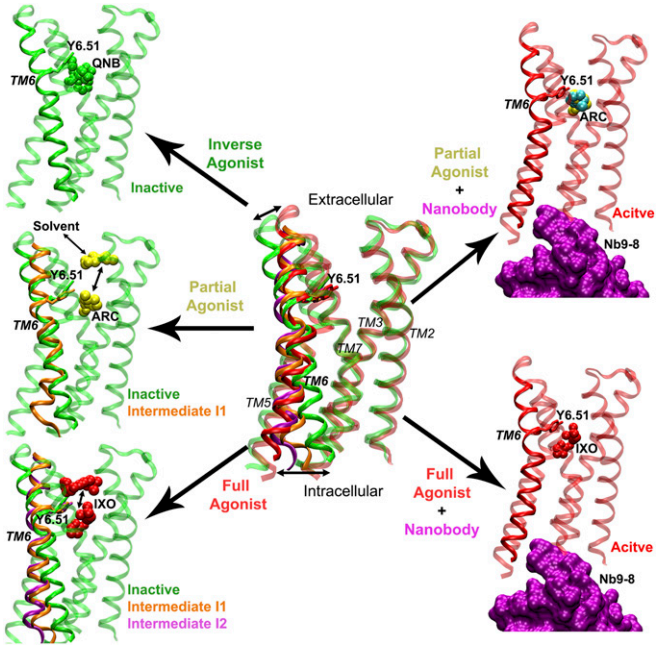

Fig. 5. Mechanism of graded activation of the M_2 muscarinic GPCR. The M_2 receptor (ribbons) samples a large conformational space with significant structural rearrangements, especially for the TM6 helix. Binding of the inverse agonist QNB (green spheres) confines the receptor in the inactive state. Without the G protein or mimetic nanobody, the partial agonist ARC (yellow spheres) biases the M_2 receptor to visit an intermediate state I1 (orange ribbons). ARC is able to dissociate completely to the bulk solvent via the extracellular vestibule and rebinds to the receptor repeatedly during a 2,030-ns GaMD simulation. In comparison, the full agonist IXO (red spheres) biases the receptor further, sampling both intermediate I1 (orange ribbons) and I2 (purple ribbons). IXO escapes out of the orthosteric pocket and visits the extracellular vestibule in one of the GaMD simulations. By adding the G-protein mimetic nanobody (purple surface), the M_2 receptor is stabilized in the fully active state (red ribbons) as bound by IXO or ARC, although ARC adopts two alternative conformations in the orthosteric pocket, ARC-P1 (yellow spheres) and ARC-P1′ (cyan spheres).

(Fig. 4 and Movie S1). A pathway connecting the orthosteric site, the center of the extracellular vestibule, and the ECL2/ECL3 opening appears to be energetically favorable for ligand dissociation and binding (Fig. 4*I*). This route has also been identified as the dominant pathway for drug binding to the β_2AR (28). Therefore, it may be a common pathway adopted by class A GPCRs for ligand recognition, although this may also depend on structural arrangement of the receptor extracellular domains and ligand size and chemical properties. For the M_2 receptor, it is worth investigating the binding of more ligands and associated receptor dynamics in the future, e.g., the *N*-methylscopolamine and atropine inverse agonists (16), the pilocarpine and McN-A343 partial agonists that elicit more consistent partial response of the M_2 receptor (16, 20), etc. In this context, although ligand dissociation from β_2AR was simulated in a previous random acceleration MD (RAMD) study (29), it was difficult to capture rebinding of the ligand. The ligand was observed to exit with similar probability via the ECL2/ECL3 and ECL2/TM2/TM7 openings, but the RAMD simulations could not differentiate the two pathways energetically. Another steered MD study on ligand dissociation from the β-ARs also suggested the two routes "may serve indistinguishably for ligand entry and exit" (ref. 30, p. 6). Although free energy profiles were obtained from the steered MD simulations, the ligand was constrained to predetermined CAVER channels, which may not reflect the real pathways as observed in cMD simulations (28). In comparison, GaMD provides unconstrained

enhanced sampling and allows for free ligand diffusion. The simulation-derived free energy profiles can be used to characterize the ligand pathways quantitatively. Notably, the orthosteric pocket and extracellular vestibule were calculated as two low-energy binding sites of ARC. This finding is consistent with previous binding assay experiments, suggesting that several partial agonists have two or more binding sites in the M_2 receptor (16, 31). Earlier computational studies also identified the extracellular vestibule as a metastable site during binding of orthosteric ligands to the M_2 and M_3 muscarinic receptors (5, 11). Therefore, GaMD is well suited for investigating ligand binding and dissociation of GPCRs and other large biomolecules. With continuing computing advances and method development, sufficient sampling of biomolecular conformations and ligand pathways may become increasingly useful for drug discovery.

Methods

GaMD simulations were performed on the M_2 muscarinic receptor that is bound by the full agonist IXO, the partial agonist ARC, and the inverse agonist QNB, in the presence or absence of the G-protein mimetic nanobody Nb9-8. For each of the receptor complexes, initial energy minimization, thermalization, and 100-ns cMD equilibration were performed using NAMD2.10 (32). Using the NAMD output structure, along with the system topology and CHARMM36 (33) force-field files, ParmEd was used to convert the simulation files into the AMBER format (34). The GaMD module implemented in the graphics processing unit (GPU) version of AMBER14 (19, 34) was then applied to perform GaMD simulation, which included 10-ns short cMD simulation used to collect potential statistics for calculating the GaMD acceleration parameters, 50-ns equilibration after adding the boost potential, and finally multiple independent GaMD production runs with randomized initial atomic velocities. The simulation frames were saved every 0.1 ps for analysis. The GaMD production simulations performed on the different M_2 receptor systems at 400-ns to 2,030-ns lengths (total ~19 μs) are listed in Table S1. Details of the GaMD simulations, energetic reweighting, system setup, and simulation analysis are provided in *SI Methods*.

ACKNOWLEDGMENTS. The authors thank Lei Huang for assistance with calculating the general automated atomic model parameterization ligand force-field parameters and Roger Sunahara, Andrew Kruse, Yu-ming Huang, and Giulia Palermo for valuable discussions. Computing time was provided on the Gordon, Comet, and Stampede supercomputers through Extreme Science and Engineering Discovery Environment Awards TG-MCA93S013 and TG-MCB140011 and on the Hopper and Edison supercomputers through National Energy Research Scientific Computing Center Project M1395, as well as on the GPU clusters at San Diego Computing Center. This work was supported by National Science Foundation Grant MCB1020765, NIH Grant GM31749, the Howard Hughes Medical Institute, and the National Biomedical Computation Resource.

1. Venkatakrishnan AJ, et al. (2013) Molecular signatures of G-protein-coupled receptors. *Nature* 494(7436):185–194.
2. Kobilka B (2013) The structural basis of G-protein-coupled receptor signaling (Nobel Lecture). *Angew Chem Int Ed Engl* 52(25):6380–6388.
3. Miao Y, McCammon JA (2016) G-protein coupled receptors: Advances in simulation and drug discovery. *Curr Opin Struct Biol* 41:83–89.
4. Deupi X, Kobilka BK (2010) Energy landscapes as a tool to integrate GPCR structure, dynamics, and function. *Physiology* 25(5):293–303.
5. Kruse AC, et al. (2012) Structure and dynamics of the M3 muscarinic acetylcholine receptor. *Nature* 482(7386):552–556.
6. Dror RO, et al. (2011) Activation mechanism of the β2-adrenergic receptor. *Proc Natl Acad Sci USA* 108(46):18684–18689.
7. Shan J, Khelashvili G, Mondal S, Mehler EL, Weinstein H (2012) Ligand-dependent conformations and dynamics of the serotonin 5-HT(2A) receptor determine its activation and membrane-driven oligomerization properties. *PLoS Comput Biol* 8(4):e1002473.
8. Provasi D, Artacho MC, Negri A, Mobarec JC, Filizola M (2011) Ligand-induced modulation of the free-energy landscape of G protein-coupled receptors explored by adaptive biasing techniques. *PLoS Comput Biol* 7(10):e1002193.
9. Li J, Jonsson AL, Beuming T, Shelley JC, Voth GA (2013) Ligand-dependent activation and deactivation of the human adenosine A(2A) receptor. *J Am Chem Soc* 135(23):8749–8759.
10. Niesen MJM, Bhattacharya S, Vaidehi N (2011) The role of conformational ensembles in ligand recognition in G-protein coupled receptors. *J Am Chem Soc* 133(33):13197–13204.
11. Kappel K, Miao Y, McCammon JA (2015) Accelerated molecular dynamics simulations of ligand binding to a muscarinic G-protein-coupled receptor. *Q Rev Biophys* 48(4):479–487.
12. Miao Y, Nichols SE, Gasper PM, Metzger VT, McCammon JA (2013) Activation and dynamic network of the M2 muscarinic receptor. *Proc Natl Acad Sci USA* 110(27):10982–10987.
13. Haga K, et al. (2012) Structure of the human M2 muscarinic acetylcholine receptor bound to an antagonist. *Nature* 482(7386):547–551.
14. Kruse AC, et al. (2013) Activation and allosteric modulation of a muscarinic acetylcholine receptor. *Nature* 504(7478):101–106.
15. Ballesteros JA, Weinstein H (1995) Integrated methods for the construction of three-dimensional models and computational probing of structure-function relations in G protein-coupled receptors. *Methods Neurosci* 25:366–428.
16. Redka DS, Heerklotz H, Wells JW (2013) Efficacy as an intrinsic property of the M(2) muscarinic receptor in its tetrameric state. *Biochemistry* 52(42):7405–7427.
17. DeVree BT, et al. (2016) Allosteric coupling from G protein to the agonist-binding pocket in GPCRs. *Nature* 535(7610):182–186.
18. Warne T, et al. (2011) The structural basis for agonist and partial agonist action on a β(1)-adrenergic receptor. *Nature* 469(7329):241–244.
19. Miao Y, Feher VA, McCammon JA (2015) Gaussian accelerated molecular dynamics: Unconstrained enhanced sampling and free energy calculation. *J Chem Theory Comput* 11(8):3584–3595.
20. McKinney M, Miller JH, Gibson VA, Nickelson L, Aksoy S (1991) Interactions of agonists with M2 and M4 muscarinic receptor subtypes mediating cyclic AMP inhibition. *Mol Pharmacol* 40(6):1014–1022.
21. Ester M, Kriegel H-P, Sander J, Xu X (1996) A density-based algorithm for discovering clusters in large spatial databases with noise. *Data Min Knowl Discov* 96(34):226–231.
22. Miao Y, et al. (2014) Improved reweighting of accelerated molecular dynamics simulations for free energy calculation. *J Chem Theory Comput* 10(7):2677–2689.
23. Dror RO, et al. (2013) Structural basis for modulation of a G-protein-coupled receptor by allosteric drugs. *Nature* 503(7475):295–299.
24. Ehlert FJ (1985) The relationship between muscarinic receptor occupancy and adenylate cyclase inhibition in the rabbit myocardium. *Mol Pharmacol* 28(5):410–421.
25. Redka DS, et al. (2014) Coupling of g proteins to reconstituted monomers and tetramers of the M2 muscarinic receptor. *J Biol Chem* 289(35):24347–24365.
26. Hughes TS, et al. (2012) Ligand and receptor dynamics contribute to the mechanism of graded PPARγ agonism. *Structure* 20(1):139–150.
27. Xu F, et al. (2011) Structure of an agonist-bound human A2A adenosine receptor. *Science* 332(6027):322–327.
28. Dror RO, et al. (2011) Pathway and mechanism of drug binding to G-protein-coupled receptors. *Proc Natl Acad Sci USA* 108(32):13118–13123.
29. Wang T, Duan Y (2009) Ligand entry and exit pathways in the beta2-adrenergic receptor. *J Mol Biol* 392(4):1102–1115.
30. González A, Perez-Acle T, Pardo L, Deupi X (2011) Molecular basis of ligand dissociation in β-adrenergic receptors. *PLoS One* 6(9):e23815.
31. Bock A, et al. (2014) Dynamic ligand binding dictates partial agonism at a G protein-coupled receptor. *Nat Chem Biol* 10(1):18–20.
32. Phillips JC, et al. (2005) Scalable molecular dynamics with NAMD. *J Comput Chem* 26(16):1781–1802.
33. Vanommeslaeghe K, MacKerell AD, Jr (2015) CHARMM additive and polarizable force fields for biophysics and computer-aided drug design. *Biochim Biophys Acta* 1850(5):861–871.
34. Case D, et al. (2014) Amber 14 (University of California, San Francisco).
35. Humphrey W, Dalke A, Schulten K (1996) VMD: Visual molecular dynamics. *J Mol Graph* 14(1):33–38, 27–28.
36. Friesner RA, et al. (2004) Glide: A new approach for rapid, accurate docking and scoring. 1. Method and assessment of docking accuracy. *J Med Chem* 47(7):1739–1749.
37. Huang L, Roux B (2013) Automated force field parameterization for nonpolarizable and polarizable atomic models based on ab initio target data. *J Chem Theory Comput* 9(8):3543–3556.
38. Roe DR, Cheatham TE, 3rd (2013) PTRAJ and CPPTRAJ: Software for processing and analysis of molecular dynamics trajectory data. *J Chem Theory Comput* 9(7):3084–3095.